

Spin-resolved electron-impact excitation of the  $6s6p$  ( $J=1$ ) states in mercury

F. Jüttemann and G. F. Hanne

*Physikalisches Institut, Universität Münster, Wilhelm-Klemm-Straße 10, 48149 Münster, Germany*

O. Zatsarinny and K. Bartschat

*Department of Physics and Astronomy, Drake University, Des Moines, Iowa 50311, USA*

(Received 27 January 2009; published 28 April 2009)

Results of angle-integrated Stokes-parameter measurements for spin-polarized electron-impact excitation of the  $6s6p$  ( $J=1$ ) states in mercury, resulting in 185 and 254 nm radiations, are presented. Due to the intermediate-coupling nature of the two states, exchange effects are visible in both excitation processes. However, their influence on the excitation of the 185 nm line ( $^1P_1 \rightarrow ^1S_0$ ) is significant only for energies very close to the excitation threshold of 6.7 eV, whereas exchange is still relevant for the 254 nm line ( $^3P_1 \rightarrow ^1S_0$ ) up to at least 50 eV incident energy. Comparison of the experimental data with theoretical predictions reveals a considerable improvement obtained through a fully relativistic 36-state Dirac  $R$ -matrix (close-coupling) model over a previous 5-state semirelativistic Breit-Pauli  $R$ -matrix approach. The experimental results at energies above 15 eV for the 254 nm line are likely dominated by cascade effects.

DOI: [10.1103/PhysRevA.79.042712](https://doi.org/10.1103/PhysRevA.79.042712)

PACS number(s): 34.80.Dp

## I. INTRODUCTION

The study of spin-resolved electron-atom collisions reveals a variety of scattering mechanisms that are masked when spin-averaged observables are measured [1,2]. The most significant spin effects in low-energy scattering generally result from electron exchange and the spin-orbit interaction, both in the target alone and in the projectile-target interaction. Such effects are often enhanced dramatically in the vicinity of resonances, i.e., temporary negative-ion states of the collision system.

For the problem of interest for the present paper, observable exchange processes are expected to contribute to the excitation of both  $6s6p$  states with total electronic angular momentum  $J=1$  because of the intermediate-coupling nature of these states. In a simplified nomenclature, they are often labeled as “ $(6s6p) ^3P_1$ ” and “ $(6s6p) ^1P_1$ ,” thus giving only the dominant configuration and the coupled spin of the two valence electrons. These states have excitation energies of 4.89 eV ( $^3P_1$ ) and 6.7 eV ( $^1P_1$ ) above the  $^1S_0$  ground state [3]. Exchange processes for the 254 nm line were already studied by angle-integrated Stokes-parameter (light-polarization) measurements for energies close to the excitation threshold by Bartschat *et al.* [4] and Wolcke *et al.* [5]. The principal motivation for the present work was to extend these studies to higher impact energies for this line as well as to the 185 nm line ( $^1P_1 \rightarrow ^1S_0$ ).

Over the past two decades, experimental benchmark data for many electron-atom collision processes have provided a solid ground for assessing various theoretical approaches. Generally these approaches are classified as “perturbative” or “nonperturbative,” depending on whether they are based on variations in the Born series or the close-coupling expansion. In addition to advanced first-order and even second-order distorted-wave [6] methods, the convergent close-coupling (CCC) [7] and the  $R$ -matrix with pseudostates (RMPS) [8] approaches have been highly successful, particularly for light quasi-one- and quasi-two-electron targets. Numerous ex-

amples, and the corresponding references, can be found in the review by Andersen *et al.* [9] and the book by Andersen and Bartschat [2]. As a result, excitation of low-lying valence states in atomic hydrogen, helium, the light alkali metal atoms, and the light alkaline-earth metal atoms is effectively considered a solved problem for atomic collision theory.

Similar progress for more complex targets, such as the noble gases other than helium, open-shell systems, and particularly heavy atoms, has been significantly slower. This is due to the increasing importance of relativistic effects and the correlations between various shells. Only recently, the CCC and the RMPS methods were extended to fully relativistic versions [10,11]. In addition, a newly developed  $B$ -spline  $R$ -matrix (BSR) method [12–14], which provides great flexibility in the description of electron scattering from complex targets through the use of term-dependent and thus nonorthogonal orbital sets, was also extended to a fully relativistic framework. The latter Dirac-based [Dirac  $B$ -spline  $R$ -matrix (DBSR)] approach was tested for  $e$ -Cs collisions [15] and then successfully applied to the  $e$ -Au problem [16], including the excitation of states with configuration  $5d^96s^2$  [17].

In addition to studying the effect of electron exchange on the excitation of the two lowest  $J=1$  states in mercury, therefore, the purpose of the present experimental project was to provide additional benchmark data for comparison with predictions from the DBSR theory. To achieve this goal we chose to measure the angle-integrated Stokes parameters, i.e., the polarization of the emitted light independent of the direction of the scattered electrons. While even more detailed electron-photon coincidence studies might have been desirable, the count rates at energies away from threshold were found to be insufficient for such experiments.

This paper is organized as follows. After discussing some general features of the experiment in Sec. II we present a brief summary of the experimental method (Sec. III). Following an outline of the numerical approach (Sec. IV), we present and discuss our results in Sec. V.

## II. GENERAL CONSIDERATIONS

### A. Scattering geometry and observables

The excited states are studied by analyzing the polarization of the light emitted perpendicular to the direction of the incident spin-polarized electron beam. The polarization vector  $\mathbf{P}$  of the incident electrons is chosen to be perpendicular to the incoming beam and parallel to the direction of the photon observation. The angle-integrated Stokes parameters are defined as

$$P_1 = \frac{I(0^\circ) - I(90^\circ)}{I(0^\circ) + I(90^\circ)}, \quad (1)$$

$$P_2 = \frac{I(45^\circ) - I(135^\circ)}{I(45^\circ) + I(135^\circ)}, \quad (2)$$

$$P_3 = \frac{I(\sigma^-) - I(\sigma^+)}{I(\sigma^-) + I(\sigma^+)}. \quad (3)$$

Here  $I(\alpha)$  denotes the light intensity transmitted by a linear polarizer aligned at an angle  $\alpha$  with respect to the direction of the incident-electron beam, while  $I(\sigma^+)$  and  $I(\sigma^-)$  are the transmitted intensities of circularly polarized light with positive and negative helicities, respectively.

The symmetry properties and the physical importance of the angle-integrated Stokes parameters were discussed in detail by Bartschat and Blum [18]. Their basic argument is as follows: as long as parity conservation holds (a very good assumption for the current study), the angle-integrated Stokes parameters  $P_2$  ( $\eta_1$  in [18]) and  $P_3$  ( $-\eta_2$ ) must vanish unless  $|\mathbf{P}| \neq 0$ . On the other hand,  $P_1$  ( $\eta_3$ ) is nonzero in general and, in fact, does not depend on  $|\mathbf{P}|$  at all. Furthermore, even for spin-polarized electron impact ( $|\mathbf{P}| \neq 0$ ),  $P_2$  vanishes unless explicitly spin-dependent effects, such as the spin-orbit interaction, influence the scattering process. Exchange alone is insufficient, but an intermediate-coupling description of the excited state (see below) as well as resonances may result in significant nonzero values of  $P_2$ . Finally, nonzero values of  $P_3$  are mainly caused by exchange processes, thereby making this circular polarization a key parameter in the study of exchange processes.

### B. Excitation process

The wave functions of the  $6s6p$  excited states with  $J=1$  in mercury are often described in the intermediate-coupling scheme (see, for example, [19]) as

$$\Psi(^3P_1) = \alpha\Psi^0(^3P_1) + \beta\Psi^0(^1P_1), \quad (4)$$

$$\Psi(^1P_1) = \alpha\Psi^0(^1P_1) - \beta\Psi^0(^3P_1). \quad (5)$$

Here  $\Psi^0$  denotes a pure  $LS$ -coupled wave function, with  $\alpha = -0.987$  and  $\beta = 0.171$  [20] representing the mixing coefficients. Note that  $\alpha^2 + \beta^2 = 1$ .

While only an approximation to a general multiconfiguration description, which could be given in any angular momentum coupling scheme that accounts for the total electronic angular momentum, the above description is useful to

qualitatively discuss the spin effects that might be expected. To begin with, both states defined in Eqs. (4) and (5) have a triplet component. This part of the wave function contributes to excitation via exchange, thereby making the observation of spin effects through the exchange mechanism possible.

Furthermore, it is well known that exchange effects diminish with increasing energy of the projectile. (In a simple picture, electrons with vastly different speeds become more or less distinguishable.) As a result, cross sections for spin-forbidden transitions usually peak close to threshold and then fall off fast with increasing projectile energy, while spin-allowed and optically allowed transitions (such as  $^1S_0 \rightarrow ^1P_1$ ) slowly increase from threshold and reach a maximum at “intermediate” projectile energies of several times the ionization potential.

Using this general argument for the two transitions of interest for the present work, the magnitudes of the triplet coefficients suggest that the  $^1P_1$  state is affected by exchange only for energies very close to threshold. At higher energies no significant contributions from spin effects to the integrated cross sections are expected because of the increasing dominance of the singlet part. This general statement was indeed verified recently for energies as small as 15 eV by Außendorf *et al.* [21]. Only at large scattering angles were some spin effects seen, but their contribution to the angle-integrated scattering cross section is negligible. In the present work, the Stokes parameter  $P_3$ , which shows the influence of exchange directly, was therefore studied only close to the excitation threshold for the  $^1P_1$  state.

The excitation of the  $^3P_1$  state, on the other hand, is much more strongly influenced by the triplet contribution, since it represents the main part in that wave function. With increasing energy, however, its influence is expected to decrease relative to the singlet part, due to the general energy dependence of the cross sections for allowed and forbidden transitions discussed above. Hence, the small singlet part of the wave function will ultimately dominate this excitation as well. In an attempt to analyze the “crossover,” the measurement of  $P_3$  for this transition was extended to incident energies of up to 80 eV. Unfortunately, however, cascade effects are also expected to be more important for this weaker transition. As will be seen below, cascades can indeed mask the observable size of the effect to a considerable extent.

### C. Hyperfine depolarization and threshold values

The present experiment was performed on the natural isotope mixture of mercury, which contains nuclear spins of  $I=0$  (69.95%),  $I=\frac{1}{2}$  (16.87%), and  $I=\frac{1}{3}$  (13.18%) [22]. Since the measurement process averages over this mixture of nuclear spins  $I$ , this leads to a depolarization caused by the hyperfine interaction. Consequently, appropriate perturbation coefficients must be used (for details, see [5]) to account for this effect in numerical calculations. This has been done in the present work.

Another interesting issue is the expected threshold polarization ( $P_1$ ) for the lines of interest. Using the qualitative argument that no orbital angular momentum can be transferred at threshold [23], it can be shown that only the mag-

netic sublevel with  $M=0$  may be excited for a pure  $LS$ -coupled  $^1P_1$  state, while only  $M=\pm 1$  may be excited for a pure  $^3P_1$  state. As a result, the two lines would have threshold polarizations of  $P_1^{\text{th}}=+1$  (185 nm) and  $P_1^{\text{th}}=-1$  (254 nm). Hyperfine depolarization changes these values to +0.85 and -0.74. In addition, both the intermediate-coupling scheme and resonance effects may cause changes in the threshold polarizations calculated in this way. Consequently, these arguments must be taken with care, but they can be used to qualitatively explain the results. They are particularly useful to analyze experimental data in the absence of any theoretical predictions to compare with.

### III. EXPERIMENT

The experimental procedure used in the present work is similar to that of earlier studies [5]. A detailed description of the current experimental setup was given by Herting and Hanne [24]. Briefly, a spin-polarized electron beam [140 meV full width at half maximum (FWHM) energy width] is extracted from a GaAs photocathode and fired onto a beam of mercury atoms from an oven. Photons emitted during the decay of excited  $^1P_1$  and  $^3P_1$  states into the  $^1S_0$  ground state are selected by an interference filter, analyzed with a polarization filter system, and finally detected by a photomultiplier. Special care was taken to determine the analyzing power of the polarization filter for both wavelengths and to avoid depolarization by radiation trapping. The latter caution is of particular importance for the 185 nm line.

As mentioned above, symmetry reasons require  $P_2$  and  $P_3$  to be proportional to the electron polarization  $|P|$ . Since our GaAs photocathode yields  $|P|=0.28$ , the measured raw data for  $P_2$  and  $P_3$  were normalized to an electron polarization  $|P|=1$ . In addition, using both positive and negative electron polarizations by simply switching the voltage of the Pockels cell allowed us to minimize instrumental asymmetries in the data shown below.

### IV. COMPUTATIONAL MODELS

The calculations for the present work were performed using the  $R$ -matrix (close-coupling) approach. A relatively simple though quite successful model was developed and described already 25 years ago by Scott *et al.* [25]. In this model, the lowest five states of mercury, with dominant configurations  $(6s^2)^1S_0$ ,  $(6s6p)^3P_{0,1,2}$ , and  $(6s6p)^1P_1$  were closely coupled to describe the low-energy  $e$ -Hg collision process. The target description was simplified by representing the inner 78 ( $1s^2, \dots, 5d^{10}$ ) electrons by a core potential, and relativistic effects were accounted for through the one-electron terms of the Breit-Pauli (BP) Hamiltonian. Predictions from this BP-5 model, with relatively minor modifications over the years, resulted in somewhat surprisingly good agreement with a variety of very detailed experimental data [2,9]. Recent examples from our group can be found in [26].

A much more sophisticated numerical method is the DBRS approach. Being a newly developed extension of the BSR complex [14] to the fully relativistic Dirac scheme, it was described in detail in recent applications to  $e$ -Cs [15]

and  $e$ -Au [16,17] collisions. The distinguishing features of the method are (i) the ability to use term-dependent, and hence nonorthogonal, sets of one-electron Dirac spinors in the target description and (ii) having  $B$  splines as the underlying effectively complete basis to expand the wave function of the projectile. Furthermore, it is an *all-electron approach*, and hence core-valence correlation effects (such as the core polarization) can be described *ab initio*.

In the present calculations, we used the Dirac-Coulomb Hamiltonian to describe both the  $N$ -electron target and the  $(N+1)$ -electron collision systems. The total wave function for each partial-wave symmetry was constructed from four-component Dirac spinors. Note that the radial functions for the large and small components were expanded in separate  $B$ -spline bases of different orders. This allowed us to avoid the occurrence of unphysical pseudostates. We used a semiexponential grid for the  $B$ -spline knot sequence and a relatively large number (111) of splines to cover the inner region up to the  $R$ -matrix radius of 50  $a_0$ . This large number of splines was required to correctly describe the finite-size nuclear model with a Fermi potential adopted in the present work.

The present DBSR close-coupling expansion contained 36 target states with configurations  $(5d^{10}6s^2)$ ,  $(5d^{10}6s6p)$ ,  $(5d^{10}6s7s)$ ,  $(5d^{10}6s7p)$ ,  $(5d^{10}6s6d)$ ,  $(5d^{10}6s8s)$ ,  $(5d^96s^26p)$ , and  $(5d^96s^27s)$ . Note the occurrence of states with single-electron excitation out of the  $5d^{10}$  subshell. The calculations of the target wave functions were carried out in the multi-configuration Dirac-Fock (MCDF) approximation with the GRASP2K relativistic atomic-structure package [27]. In order to account for core relaxation, we used different subsets of one-electron orbitals for the  $(5d^{10}6snl)$  valence and the  $(5d^96s^2nl)$  core-excited states. This allowed us to reproduce all excitation energies with an accuracy of better than 0.15 eV. The size of the chosen close-coupling expansion was restricted by the available computational resources. Note that the  $(5d^96s^26d)$  and  $(5d^96s^24f)$  core-excited states had to be omitted from the present expansion, and this may affect the convergence of the scattering calculations. More details of the present calculations will be given in a separate paper, along with a comparison to a variety of available experimental data for low-energy near-threshold excitation.

We calculated partial-wave contributions up to  $J=41/2$  numerically and used a geometric extrapolation scheme to account for even higher partial waves if necessary. The angle-integrated Stokes parameters were then calculated in the same way as in the standard  $R$ -matrix approach. For the present work, we employed the program MJK of Grum-Grzhimailo [28].

### V. RESULTS AND DISCUSSION

Before we discuss the results in detail, we recall that the experimental data are influenced by cascade effects, i.e., the indirect population of the excited states by photon emission from higher states. The threshold for cascading in the present work is 7.7 eV, at which the  $(6s7s)^3S_1$  can be excited. Cascade effects, which are not accounted for in the calculation, tend to reduce the absolute values of the integrated Stokes parameters.

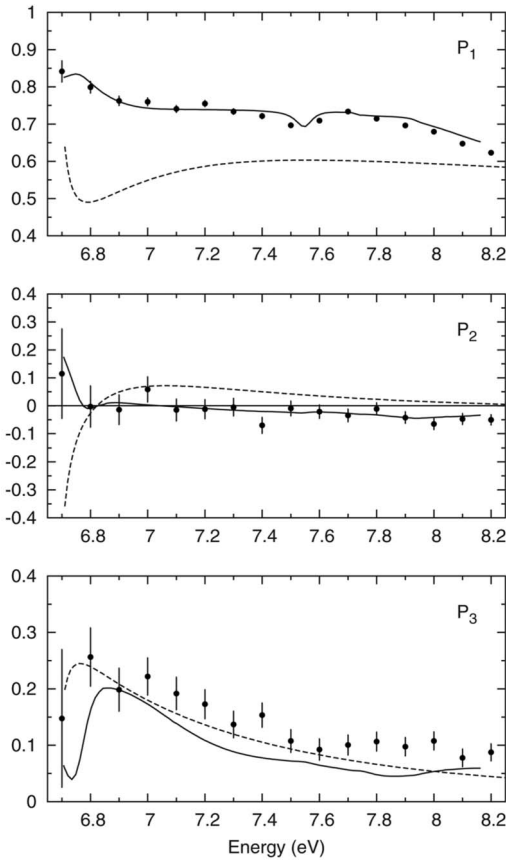


FIG. 1.  $P_1$ ,  $P_2$ , and  $P_3$  for the 185 nm line in mercury for energies close to the excitation threshold of 6.7 eV. Solid circles: experimental results; solid line: DBSR-36 calculation; dashed line: BP-5 calculation.

**A. 185 nm line ( $^1P_1 \rightarrow ^1S_0$ )**

Figure 1 shows results for  $P_1$ ,  $P_2$ , and  $P_3$  for energies close to the excitation threshold of 6.7 eV. Recall that  $P_1$  was estimated to be 0.85 at the excitation threshold in the case of pure  $LS$  coupling. Both calculations tend toward this value, although the BP-5 results drop immediately for energies just slightly above the threshold. On the other hand, the DBSR-36 predictions stay up, in essentially perfect agreement with the experimental data. Even the small dip in  $P_1$  around 7.5 eV, indicating a resonance structure associated with the onset of the aforementioned  $^3S_1$  state, is predicted very well. Since this, and the higher states, is not included in the five-state model, no structure is predicted in this case.

The near-threshold results for the angle-integrated Stokes parameters  $P_2$  and  $P_3$  in Fig. 1 are both normalized to 100% incident-electron spin polarization. It appears that the  $P_2$  values predicted by the DBSR-36 model are once again in better agreement with experiment than those from the BP-5 model. At energies above 7.5 eV, there is a tendency toward slightly negative values for  $P_2$  in both the experimental and the DBSR-36 results. This deviation from zero suggests that spin-orbit coupling affects the excitation process. The intermediate-coupling description of the excited state [see Eq. (5)], together with exchange, is likely the principal reason for these nonzero results.

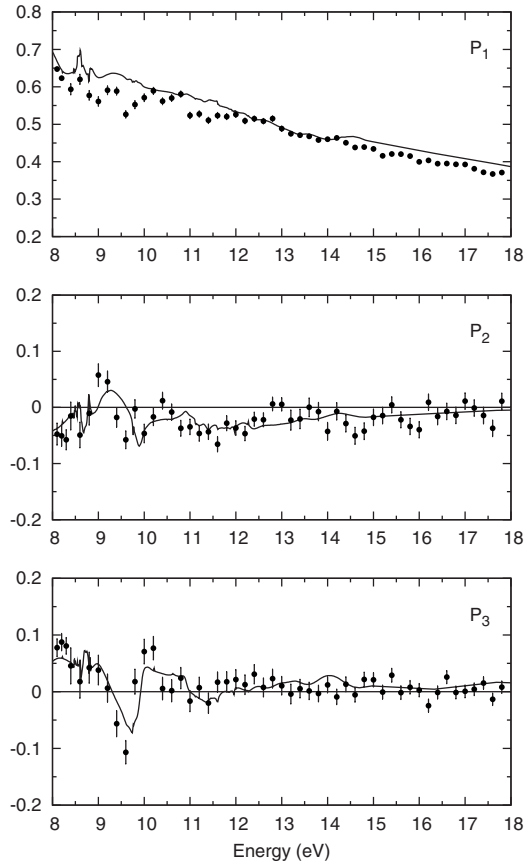


FIG. 2.  $P_1$ ,  $P_2$ , and  $P_3$  for the 185 nm line in mercury for incident energies between 8 and 18 eV. Solid circles: experimental results; solid line: DBSR-36 calculation.

The theoretical results for  $P_3$  are very similar in both models, except when very close to the excitation threshold. Overall, the agreement with the experimental data is slightly better for the older BP-5 calculation. One should keep in mind, however, the difficulty of obtaining accurate experimental data for this transition at these low energies, where the excitation cross section is very small. We carefully checked the experimental setup and are not aware of significant systematic instrumental errors. As expected, exchange is significant for scattering energies close to the excitation threshold and its influence decreases with increasing energy.

Figure 2 shows results for  $P_1$ ,  $P_2$ , and  $P_3$  for energies from 8 to 18 eV. For  $P_1$  the experiment as well as the DBSR-36 results shows a relatively steady decrease in magnitude from approximately 0.7 at 8 eV to about 0.4 at 18 eV. For the higher energies from 12 to 18 eV we notice excellent agreement between the DBSR-36 results and the experimental data with virtually no resonance structures visible. Between 8 and 12 eV however, both the experimental and the DBSR-36 results show some resonance structure. Here the experimental results lie up to 0.1 below the theoretical predictions. Note that a further extension of  $P_1$  to energies of about 165 eV was published by Herting and Hanne [24].

The spin-dependent Stokes parameters  $P_2$  and  $P_3$  in Fig. 2 are again both normalized to 100% incident-electron spin polarization. The tendency toward slightly negative values for  $P_2$  in the DBSR-36 results remains, apart from a reso-

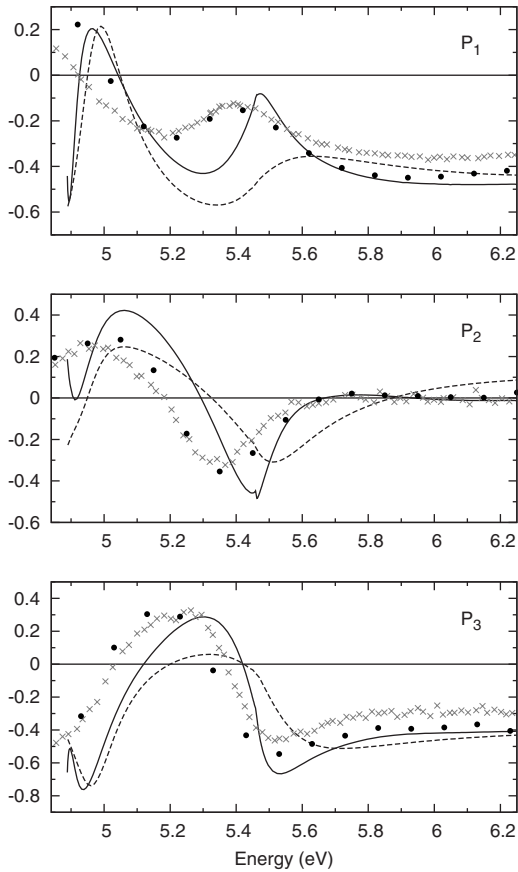


FIG. 3.  $P_1$ ,  $P_2$ , and  $P_3$  for the 254 nm line in mercury for energies close to the excitation threshold of 4.9 eV. Solid circles: present experimental results; crosses: experimental data by Wolcke *et al.* [5]; solid line: DBSR-36 calculation; dashed line: BP-5 calculation.

nance with slightly positive values around 9.3 eV. Within the experimental uncertainty, this is in good agreement with the experimental data. In the case of  $P_3$  the situation is similar in that the DBSR-36 calculation predicts mainly slightly positive values with a pronounced dip below zero at about 9.7 eV. This is again in very good agreement with the experiment. The small magnitude of the experimental data and the DBSR-36 results for  $P_3$  for energies above 11 eV suggests that exchange effects essentially vanish for incident projectile energies in excess of 11 eV.

### B. 254 nm line ( $^3P_1 \rightarrow ^1S_0$ )

Figure 3 shows results for  $P_1$ ,  $P_2$ , and  $P_3$  for energies close to the excitation threshold of 4.89 eV. Recall that  $P_1$  for this line was estimated to be  $-0.74$  at the excitation threshold in the limiting case of pure  $LS$  coupling. On the other hand, the famous  $(6s6p^2)^4P_{5/2}$  threshold resonance around 4.91 eV [29,30] would lead to a  $P_1$  value of  $+0.41$  [5]. Indeed, even after convolution with the energy width of 140 meV in the incident beam, both calculations predict a rapid change in  $P_1$  over a fraction of an eV in the incident energy, whereas the experimental data actually remain positive in this energy region. After investigating the convolution

procedure in detail, we believe that the apparent discrepancy between experiment and theory is due to both theories predicting the threshold resonance just a few meV too high.

The remaining resonance structures in  $P_1$  are at least qualitatively reproduced by both calculations, although the agreement with the experimental data, even for the DBSR-36 model, is not as good as for the 185 nm line. Again, the main reason is the fact that the theoretical positions of the  $(6s6p^2)^2D_{3/2,5/2}$  resonances are a little too high. Nevertheless, the DBSR-36 calculation still represents a clear improvement over the BP-5 model in this regard.

Note that the experimental data of Wolcke *et al.* [5] deviate from the present results by up to about 10%. We believe that the current data are more reliable due to several improvements made in the experimental setup over time.

Recall that our results for the spin-dependent Stokes parameters  $P_2$  and  $P_3$  in Fig. 3 are again both normalized to 100% incident-electron spin polarization. The DBSR-36 predictions for both light polarizations are once again in slightly better agreement with the experimental data than those from the BP-5 model. Significant nonzero values for  $P_2$  are seen between threshold and 5.6 eV. These structures in  $P_2$  are strongly correlated with the  $(6s6p^2)^2D_{3/2,5/2}$  negative-ion resonances around 5.2 and 5.5 eV, respectively.

Not surprisingly, the circular polarization  $P_3$  is also influenced by the negative-ion resonances. In particular, we note a sign reversal of the otherwise negative values for  $P_3$ . Negative  $P_3$  values are expected from exchange effects alone on the excitation process of this line, especially close to the excitation threshold. The rapid change as a function of energy is once again due to the  $(6s6p^2)^4P_{5/2}$  and  $(6s6p^2)^2D_{3/2,5/2}$  resonances around 4.9, 5.2, and 5.5 eV. Looking at Table 2 of Wolcke *et al.* [5], we see that isolated resonances with these configurations would give normalized  $P_3$  values (corresponding to  $-\eta_2/P_y$  in the above paper) of  $-0.69$ ,  $+0.52$ , and  $-0.69$ , respectively.

A further extension of  $P_2$  and  $P_3$  for energies from 6 up to 14 eV is available from earlier studies by Wolcke [31]. In order to thoroughly test the DBSR-36 predictions, we show these results in Fig. 4 together with the corresponding data for  $P_1$  by Herting and Hanne [24].

A quick glance at  $P_1$ ,  $P_2$ , and  $P_3$  for this energy range already reveals a considerable influence of numerous further negative-ion resonances. These are again correlated with significantly nonzero values of  $P_2$ . The most pronounced resonance structures are seen between 8.5 and 11.5 eV. Recommended classifications in this energy regime are mostly  $(5d^96s^26p^2)$ , though two  $(5d^{10}6s7p^2)$  configurations have also been suggested [32]. Regarding the resonance positions, we see again a tendency for the theoretical positions to be slightly too high. Given the complexity of this problem and the computational limitations on our close-coupling expansion, this is not surprising at all. In fact, at this time we are very satisfied with the way the resonance structures are reproduced in both shape and magnitude.

Moving to the individual light polarizations, we note that the differences between experiment and theory regarding the magnitude of  $P_1$  may, at least to some extent, be due to the influence of cascade effects, which are not accounted for in the calculation. Nevertheless, there is also a significant dif-

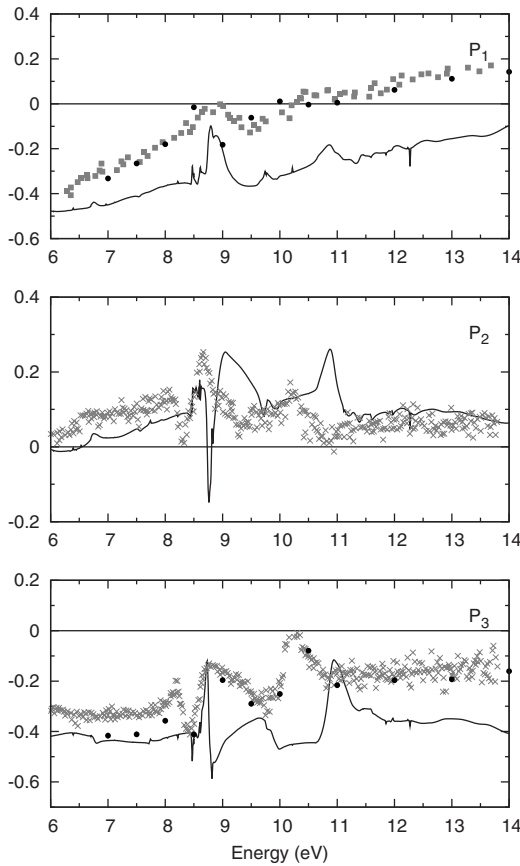


FIG. 4.  $P_1$ ,  $P_2$ , and  $P_3$  for the 254 nm line in mercury for energies from 6 up to 14 eV. Solid circles: present experimental results; squares: experimental data by Herting and Hanne [24]; crosses: experimental data by Wolcke [31]; solid line: DBSR-36 calculation.

ference in the zero crossing, which is found experimentally around 10.5 eV, while the DBSR-36 model predicts it around 19 eV (see Fig. 5).

Except for the apparent shift in the dominating resonance positions, the overall agreement between experiment and the DBSR-36 theory for  $P_2$  is good. For  $P_3$ , on the other hand, we see an increasing difference in magnitude with increasing energy. Apart from possible cascade effects (see below), it seems possible that the magnitude of the experimental data themselves may be somewhat too small. As seen from Fig. 3, the present  $P_3$  results for energies close to the excitation threshold are about 10% larger than those measured previously—in excellent agreement with the DBSR-36 predictions. The remaining small, though growing (with increasing energy) difference in the magnitude of  $P_3$  is likely due to the influence of cascade effects.

Finally, in order to study the influence of the  $\Psi^0(^3P_1)$  part of the wave function for excitation energies well above the excitation threshold, we extended the existing experimental data from incident energies of 15 eV to energies up to 80 eV. Figure 5 exhibits our results for  $P_2$  and  $P_3$ , as well as the  $P_1$  results of Herting and Hanne [24] for the aforementioned incident energy range.

The results for  $P_1$  steadily change from about +0.2 at 15 eV to  $\sim -0.05$  at 80 eV. The discrepancy between experi-

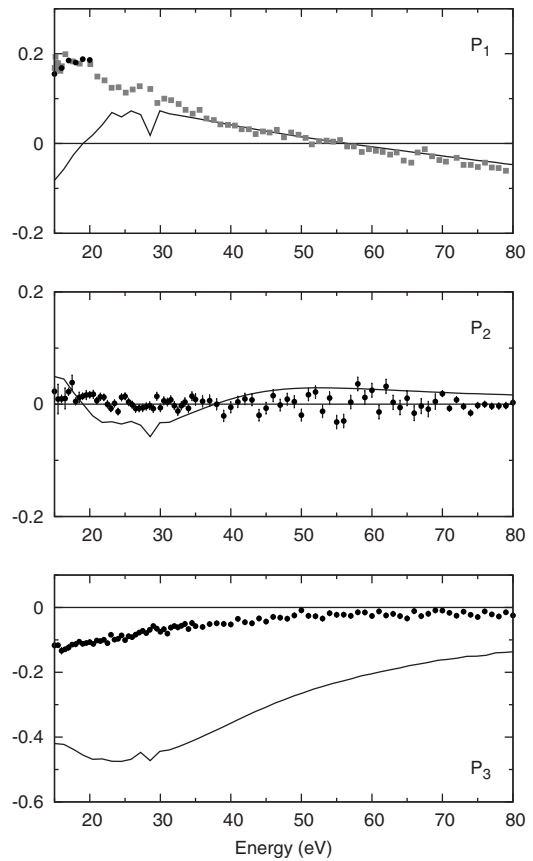


FIG. 5.  $P_1$ ,  $P_2$ , and  $P_3$  for the 254 nm line in mercury for energies from 15 up to 80 eV. Solid circles: present experimental results; squares: experimental data by Herting and Hanne [24]; solid line: DBSR-36 calculation.

ment and the DBSR-36 results for energies from 15 to about 30 eV is a direct consequence of the calculation predicting the first zero crossing in  $P_1$  several eV too high (cf. Fig. 4). For higher energies (35–80 eV), the DBSR-36 calculation achieves excellent agreement with the experimental data. This is somewhat astonishing in light of the possibility of significant cascade effects at these energies. On the other hand, good agreement with the high-energy results of Herting and Hanne [24] for  $P_1$  (for both lines) was also obtained by McConnell and Moiseiwitsch [19], who used the much simpler Born-Ochkur approximation.

Within the experimental uncertainty, the experimental data for  $P_2$  are consistent with zero. For incident energies above 35 eV, the DBSR-36 model predicts slightly positive values. Since these predictions lie within the margins of fluctuation in the experimental data points, they could be neither confirmed nor rejected by the present experiment.

The experimental data for  $P_3$ , which gradually change from about  $-12\%$  at 15 eV to  $-2\%$  at 50 eV and above, are in qualitative agreement with the general expectation of decreasing exchange effects, and consequently the weakening importance of the triplet part of the intermediate-coupling wave function, with increasing incident projectile energy. The DBSR-36 model yields a similar qualitative change in  $P_3$  above 25 eV, but it generally predicts much larger magnitudes of  $P_3$ . The very same is true for the BP-5 model (not shown).

Since it is unlikely that the theoretical models would suddenly fail with increasing projectile energy, where the description of the direct excitation process generally simplifies, the substantial deviations between theory and experiment regarding the magnitude of  $P_3$  are most likely due to a dominant effect of cascading. As mentioned above, indirect population of the initial state for the optical transition is generally expected to reduce the observed light polarization. If this is, indeed, the reason for the small observed magnitudes for  $P_3$ , it should also be expected for  $P_2$  and hence would make it even less likely to measure nonzero values for this parameter and thereby demonstrate the importance of explicitly spin-dependent interactions in this energy range.

A straightforward way to test this hypothesis is to compare experiment and theory for Stokes parameters measured in electron-photon coincidence setups, for which cascade effects are essentially negligible. Indeed, comparison of the DBSR-36 predictions for the angle-differential  $P_3$  at 15 eV shows good agreement with the BP-5 results and the experimental data obtained by Herting *et al.* [26]. Such experiments for even higher energies are currently in progress.

## VI. SUMMARY AND CONCLUSIONS

In this paper, we presented results for spin-polarized electron-impact excitation of the 185 and 254 nm spectral

lines in mercury, for incident energies between threshold and 80 eV. In the near-threshold regime, a fully relativistic 36-state DBSR approach with nonorthogonal orbital sets provided very satisfactory agreement with the experimental data and represented a substantial improvement over an earlier 5-state semirelativistic Breit-Pauli model. At higher energies, the experimental data are in qualitative agreement with the expected reduction of exchange effects with increasing energy. Furthermore, relativistic effects are insufficient to cause significant deviations of the linear polarization  $P_2$  from zero. Unfortunately, cascade effects seem particularly strong for the spin-dependent light polarizations of the 254 nm line, thereby making a straightforward study of exchange effects virtually impossible. The latter problem can, in principle, be addressed by performing an electron-photon coincidence experiment. While technically very challenging, efforts along this direction are currently in progress.

## ACKNOWLEDGMENTS

This work was supported, in part, by the Deutsche Forschungsgemeinschaft (F.J. and G.F.H.) and by the United States National Science Foundation under Grants No. PHY-0555226 and No. PHY-0757755 (O.Z. and K.B.).

- 
- [1] J. Kessler, *Polarized Electrons*, 2nd ed. (Springer-Verlag, New York, 1985).
- [2] N. Andersen and K. Bartschat, *Polarization, Alignment, and Orientation in Atomic Collisions* (Springer-Verlag, New York, 2001).
- [3] Y. Ralchenko, A. E. Kramida, J. Reader, and NIST ASD Team, NIST Atomic Spectra Database, version 3.1.4, 2008, <http://physics.nist.gov/asd3>
- [4] K. Bartschat, G. F. Hanne, and A. Wolcke, *Z. Phys. A* **304**, 89 (1982).
- [5] A. Wolcke, K. Bartschat, K. Blum, H. Borgmann, G. F. Hanne, and J. Kessler, *J. Phys. B* **16**, 639 (1983).
- [6] D. H. Madison, I. Bray, and I. E. McCarthy, *J. Phys. B* **24**, 3861 (1991).
- [7] I. Bray, D. V. Fursa, A. S. Kheifets, and A. T. Stelbovics, *J. Phys. B* **35**, R117 (2002).
- [8] K. Bartschat, E. T. Hudson, M. P. Scott, P. G. Burke, and V. M. Burke, *J. Phys. B* **29**, 2875 (1996).
- [9] N. Andersen, K. Bartschat, J. T. Broad, and I. V. Hertel, *Phys. Rep.* **279**, 251 (1997).
- [10] D. V. Fursa and I. Bray, *Phys. Rev. Lett.* **100**, 113201 (2008).
- [11] N. R. Badnell, *J. Phys. B* **41**, 175202 (2008).
- [12] O. Zatsarinny and C. Froese Fischer, *J. Phys. B* **33**, 313 (2000).
- [13] O. Zatsarinny and K. Bartschat, *J. Phys. B* **37**, 2173 (2004).
- [14] O. Zatsarinny, *Comput. Phys. Commun.* **174**, 273 (2006).
- [15] O. Zatsarinny and K. Bartschat, *Phys. Rev. A* **77**, 062701 (2008).
- [16] M. Maslov, M. J. Brunger, P. J. O. Teubner, O. Zatsarinny, K. Bartschat, D. V. Fursa, I. Bray, and R. P. McEachran, *Phys. Rev. A* **77**, 062711 (2008).
- [17] O. Zatsarinny, K. Bartschat, M. Maslov, M. J. Brunger, and P. J. O. Teubner, *Phys. Rev. A* **78**, 042713 (2008).
- [18] K. Bartschat and K. Blum, *Z. Phys. A* **304**, 85 (1982).
- [19] J. C. McConnell and B. L. Moisewitsch, *J. Phys. B* **1**, 406 (1968).
- [20] A. Lurio, *Phys. Rev.* **140**, A1505 (1965).
- [21] G. Außendorf, F. Jüttemann, K. Mukhtavat, L. Sharma, R. Srivastava, A. D. Stauffer, K. Bartschat, D. V. Fursa, I. Bray, and G. F. Hanne, *J. Phys. B* **39**, 4435 (2006).
- [22] P. De Bievre and P. D. P. Taylor, *Int. J. Mass Spectrom. Ion Phys.* **123**, 149 (1993).
- [23] I. C. Percival and M. J. Seaton, *Philos. Trans. R. Soc. London, Ser. A* **251**, 113 (1958).
- [24] C. Herting and G. F. Hanne, *J. Phys. B* **35**, L91 (2002).
- [25] N. S. Scott, P. G. Burke, and K. Bartschat, *J. Phys. B* **16**, L361 (1983).
- [26] C. Herting, G. F. Hanne, K. Bartschat, A. N. Grum-Grzhimailo, K. Mukhtava, R. Srivastava, and A. D. Stauffer, *J. Phys. B* **35**, 4439 (2002).
- [27] P. Jönsson, X. He, C. Froese Fischer, and I. P. Grant, *Comput. Phys. Commun.* **177**, 597 (2007).
- [28] A. N. Grum-Grzhimailo, *Comput. Phys. Commun.* **152**, 101 (2003).
- [29] N. M. Erdevdi, O. B. Shpenik, and V. S. Vukstich, *Opt. Spectrosc.* **95**, 529 (2003).
- [30] J. P. Sullivan, P. D. Burrow, D. S. Newman, K. Bartschat, J. A. Michejda, R. Panajotovic, M. Moghbelalhossein, R. P. McEachran, and S. J. Buckman, *New J. Phys.* **5**, 159 (2003).
- [31] A. Wolcke, Ph.D. thesis, Physikalisches Institut, Universität Münster, 1984.
- [32] S. J. Buckman and C. W. Clark, *Rev. Mod. Phys.* **66**, 539 (1994).